Synthesis and Structural Design of Co, Ni-free Disorder Rock-Salt Cathode Materials for Lithium-ion Batteries Via Novel Mechanochemical Ball Milling Method

AUTHOR: Abdulrahman Hamdy Abdulrasoul Mahgoub Hassan Elsharkawy - 10771090

ADVISOR: Professor Jie Li

ACADEMIC YEAR: 2022-2023

1. Introduction

The need for renewable energy-powered rechargeable batteries is increasing steadily as cities aim to reduce carbon emissions, especially in relation to vehicle operations. Among various battery technologies, lithium-ion batteries (LIBs) remain the most suitable option due to their superior overall performance [1]. Cathode materials, compared to anode materials, pose a challenge for achieving higher energy densities in lithium-ion batteries (LIBs) due to their relatively lower specific capacities. Consequently, advancing the development of cathode materials serves as the primary strategy for further improving the energy density of LIBs [2]. In recent years, there has been significant research interest in a novel category of cathodes called cation disordered rock salt (DRX) cathodes. These materials have garnered attention due to their reasonable lithium transportation properties, despite the absence of an ordered layered structure commonly found in traditional cathode materials [3]. The transportation of lithium ions in DRX materials is facilitated by a network of percolating 0-TM transport channels that become active once a specific lithium threshold is reached. This discovery has prompted extensive exploration of potential synergies among different transition metals, thereby inspiring the development of new cathode chemistries [4]. The synthesis method of DRX materials has received limited attention, and there is a lack of research focused on finding an easy and efficient approach to achieve the desired phase and enhance performance. In this study, a novel synthesis technique employing dry ball milling is introduced as a simple, cost-effective, and energy-efficient method for producing DRX cathodes with a stoichiometry of $Li_{1.25}Fe_{0.5}Nb_{0.25}O_2$. Additionally, cation deficiency engineering is explored in this study to try to optimize the overall electrochemical performance of the DRX cathodes.

2. Objectives

The main goal is to identify a simple and efficient method for synthesizing DRX materials. In pursuit of this objective, the utilization of mechanochemical milling as an alternative to conventional synthesis methods was investigated. Mechanochemical milling involves mechanically activating the materials through grinding or milling, which induces chemical transformations at the molecular level. This approach offers several advantages, including simplicity, accessibility, cost-effectiveness, energy efficiency, and environmental friendliness. Another important objective is to improve the performance of DRX materials by introducing cation vacancies using the high-energy ball milling technique.

3.   Experimental Section

Material Preparation

The synthesis process of $Li_{1.25}Fe_{0.5}Nb_{0.25}O_2$, $Li_{1.2}Fe_{0.5}Nb_{0.26}O_2$, and $Li_{1.1}Fe_{0.5}Nb_{0.28}O_2$ compounds with 0%, 2%, and 6% cation vacancies, respectively, is via mechanochemical ball milling. Stoichiometric amounts of Nb_2O_5, Fe_2O_3, and Li_2O (with 10 wt% excess of Li_2O to compensate for lithium loss during synthesis) were employed as precursors. These precursors were dispersed in Ar-filled zirconium jars and then subjected to planetary ball milling at different rotational speeds and durations as per the experimental plan. Each jar contained ≈2.5 g of total precursor material, and the grinding media consisted of 16 large (10 mm diameter), 15 medium (5 mm diameter), and 15 small (3 mm diameter) zirconium balls, resulting in a balls-to-materials weight ratio of approximately 23:1.

To prepare the carbon composite samples $Li_{1.25}Fe_{0.5}Nb_{0.25}O_2/C$, $Li_{1.2}Fe_{0.5}Nb_{0.26}O_2/C$, and $Li_{1.1}Fe_{0.5}Nb_{0.28}O_2/C$, the as prepared samples were mixed with carbon black in a weight ratio of 90:10 wt% using a planetary ball mill at a speed of 750 rpm for a duration of 4 hours. The mixing process was carried out in zirconium jars, utilizing zirconium balls as the griding media with a weight of 10~15 times that of the material.

Electrochemical Measurement

To prepare the positive electrode, a mixture containing 80 wt% of active material, 10 wt% of carbon black, and 10 wt% of 5% wt polyvinylidene fluoride (PVDF) that was dissolved in N-methyl-2-pyrrolidone (NMP) was subjected to planetary ball mill at a speed of 250 rpm for a duration of 2 hours. This mixture was then pasted onto an aluminum (Al) foil current collector. Subsequently, the electrode was subjected to overnight drying in a vacuum oven maintained at 120°C. The coin cell assembly process was performed within an argon-filled glove box and tested under room temperature between 1.5V and 4.8V.

As part of the electrochemical measurements, a charge/discharge test was performed to evaluate the performance of the battery, such as capacity retention, energy efficiency, and cycling stability. Additionally, the differential (dQ/dV) curve analysis was utilized to gain further understanding of phenomena such as redox reactions, phase transitions, and the dynamics of the electrode/electrolyte interface.

Materials characteristics

The X-ray diffraction (XRD) patterns were obtained using a powder X-ray diffractometer to identify the present of crystallinity and detect impurities. The Scanning Electron Microscopy (SEM) images were collected with a scanning electron microscope (Carl Zeiss AURIGA) to analyze the size and morphology of nanoparticles. Moreover, energy dispersive X-ray (EDX) element mapping was performed to analyze the elemental composition of cathode material and map their elemental distributions.

4.   Results and discussion

The aim is to contribute to the development of sustainable and energy-efficient material synthesis techniques through the optimization of mechanochemical ball milling parameters including rotational speed, milling time, the presence or absence of a reverse rotation, the number of stops during the process, and the weight ratio between balls and materials.

4.1.   The material with 0% cation vacancies

The synthesis of $Li_{1.25}Fe_{0.5}Nb_{0.25}O_2$, referred to as the material with 0% cation vacancies, was carried out through dry milling. The preparation process focused on optimizing the rotational speed and milling time while keeping the other parameters constant.
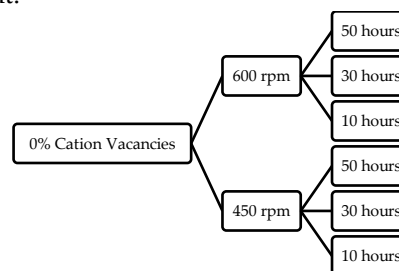

Figure 1 Optimization process plan for synthesizing the 0% cation vacancies cathode material via dry milling.

The charge/discharge curves and corresponding dQ/dV curves of the 0% cation vacancies materials synthesized with different dry milling parameters are shown in figure 2. With a voltage range between 1.5 V and 4.8 V, figure 2a shows the charge/discharge curves of the material with 0%

cation vacancies at rotational speed of 600 rpm running for a duration of 50 hours (left) and 10 hours (right). The milling machine stops for a 20-minute rest after every 1 hour of dry milling.

The initial observation is that the 10 hour material exhibits a lower charge and discharge capacities compared to the 50 hour material. Furthermore, during the initial charge, the Fe oxidation portion (O1) appears to be shorter, while the oxygen oxidation portion (O2) appears to be relatively longer in the 10 hour material compared to the 50 hour material. This can be attributed to the shorter milling time that is not sufficient to achieve the desiered disorder rock salt phase.
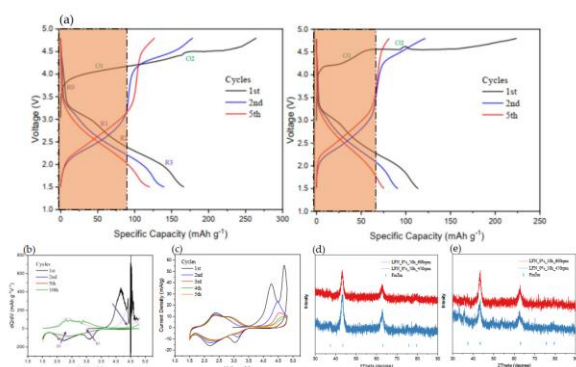

Figure 2 (a) Charge/discharge curves of the 0% cation vacancies material with different milling time. (b) The dQ/dV curve of 0%-600 rpm-50 hour material. (c) The CV of 0%-600 rpm-50 hour material. (d) The XRD patterns of the 0% cation vacancies material at different rotational speeds and milling time

Furthermore, the contribution of Fe^{2+}/Fe^{3+} redox reactions in the second charge indicated by the shaded area is lower for the 10 hours material compared to the 50 hours material. This suggests that the 10 hours milling process does not fully activate the Fe redox reactions supporting the notion that insufficient milling time affects the activation of transition metal redox processes, resulting in diminished electrochemical performance.

The dQ/dV curve of the 0%-600 rpm-50 hour material depicted in figure 2b demonstrates various electrochemical redox reactions. These include the oxidation and reduction reactions of Fe (O1 and R3), as well as the oxidation and reduction reactions of oxygen (O2, R1 and R2). Over cycling, discharge plateaus R1 and R2 display a rapid decrease in their peaks, indicating the irreversible nature of the oxygen reduction reaction. Furthermore, the peak corresponding to the discharge plateau R3, which represents the reduction reaction of Fe, shows also significant decline over cycling highlighting the irreversibility

of the Fe redox reaction which explains the capacity fade observed during cycling. Similarly, the oxidation peaks show a decreasing trend over cycling, indicating the poor reversibility of oxygen redox.

To assess the impact of oxygen redox on the electrochemical behavior of the cathode material during cycling, cyclic voltammetry (CV) was conducted on the 0%-600 rpm-50 hour material. Figure 2c depicts the cyclic voltammogram recorded between 1.5V and 4.8V. The CV curve exhibits two anodic peaks centered around 4.2V and 4.8V, indicating the occurrence of an Fe and oxygen oxidation reactions respectively. Similarly, two cathodic peaks observed around 2.15 V and 3V, representing the corresponding Fe and oxygen reduction processes respectively. During cycling, the intensity of the oxygen oxidation peak at the 4.8V and the oxygen reduction peak at 3 V exhibit a notable decrease, indicating the poor reversibility of the oxygen redox reactions, as previously mentioned. Additionally, the Fe oxidation peak observed at 4.2 V, continues to shift towards higher voltages and decreases in intensity over cycling. Similarly, the Fe reduction peak located at 2.15 V, also experiences a decrease in intensity. These reductions in peak intensity, accompanied by a decrease in current density, are indicative of hysteresis, voltage fade, and capacity fade occurring in the system.

Figures 2d and e illustrate the XRD patterns of the material with 0% cation vacancies at various milling times and rotational speeds. Upon examining the 50-hour samples, it is evident that the intensity of the first peak at approximately 37 degrees is considerably weak, indicating poor crystallization. This lack of crystallization can be attributed to the absence of calcination in the synthesis process. Furthermore, some impurities are also detected, particularly in the 10-hour samples. Specifically, in the 0%-450 rpm-10 hour material, two peaks are observed at around 50 and 54 degrees, which correspond to impure phases which can be attributed to the reaction between LiO and Nb_2O_5, resulting in the formation of $LiNbO_3$. However, by increasing the milling speed and, more significantly, prolonging the milling duration, it appears that the formation of $LiNbO_3$ can be prevented, as there are no peaks observed around 50 and 54 degrees. This indicates a progression towards the desired phase. In

conclusion, increasing the milling time helps to minimize the presence of impure phases.
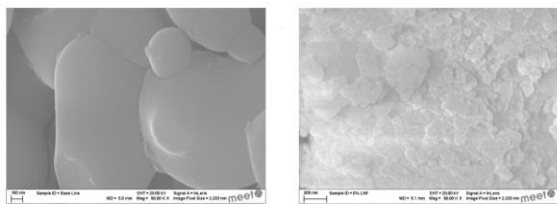

Figure 3 The SEM images for the base line material after calcination (left) and the SEM images for the 0%-450 rpm-50 hour material (right).

In Figure 3, a comparison between the 0%-450 rpm-50 hour material and the baseline material after calcination. Several observations can be made based on these SEM images:

-       Particle Size: The particles in the 0%-450 rpm-50 hour material appears to be much smaller compared to the baseline material after calcination representing improved performance, as smaller particles tend to have larger surface areas and enhanced reactivity.

-       Agglomeration: The dry milling process in the 0%-450 rpm-50 hour material leads to a significant degree of agglomeration. On the other hand, calcination results in a better distribution of particles. The good particle distribution achieved after calcination is favorable for achieving a homogeneous distribution of active materials during the slurry preparation process. In contrast, the agglomeration of particles in the 0%-450 rpm-50 hour material makes it more challenging to achieve a homogeneous slurry.

4.2. The materials with 2% and 6% cation vacancies

To improve the electrochemical performance of DRX cathodes, this thesis focuses on introducing cation vacancies using mechanochemical milling as the chosen synthesis strategy. Cation vacancies were introduced by intentionally creating a deficiency of lithium (Li) ions while increasing the amount of niobium (Nb) to compensate for the reduced Li content.

2% cation vacancies

To optimize the preparation of the 2% cation vacancies ($Li_{1.2}Fe_{0.5}Nb_{0.26}O_2$) through dry milling, a projected plan in figure 1 was followed similar to the 0% cation vacancies.
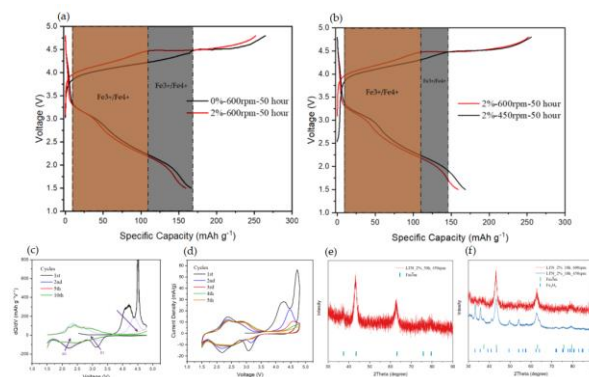

Figure 4 (a) Charge/discharge curves of the initial cycle of the 0%-600 rpm-50 hour and 2%-600 rpm-50 hour. (b) Charge/discharge curves of the initial cycle of the 2%-600 rpm-50 hour and 2%-450 rpm-50 hour. (c) The dQ/dV curve of 2%-450 rpm-50 hour material. (d) The CV of 2%-450 rpm-50 hour material. (e) and (f) The XRD patterns of the 2% cation vacancies material at different rotational speeds and milling time.

During the initial charge of the 2%-600 rpm-50 hour material, an oxidation plateau is observed above 4.1 V, representing the oxidation of Fe^{3+} to Fe^{4+} indicated by the orange shaded area in figure 4a. However, this oxidation process of Fe is relatively shorter compared to the material with 0% cation vacancies. This short plateau is due to the presence of more impurities. Moreover, another oxidation plateau at 4.5V is observed to be longer than that of the material with 0% cation vacancies indicating the higher participation of oxygen in the redox reaction.

After noticing the poor performance from the 10 hour material, in this case the 50 hour milling time was kept fixed while changing the rotational speed from 600 rpm to 450 rpm. Figure 4b shows the first charge and discharge of the materials with 2% cation vacancies at different rotational speeds. In the first charge the 2%-450 rpm-50 hour material, the oxidation plateau of Fe is relatively longer compared to the 2%-600 rpm-50 hour material. This means that the 2%-450 rpm-50 hour material has a higher proportion of Fe participating in the redox reaction, indicating the presence of more pure phases compared to the 2%-600 rpm-50 hour material.

The dQ/dV the 2%-450 rpm-50 hour material, as shown in figure 4c, provides insights into the oxidation (O1 and O2) and reduction (R1, R2, and R3) reactions of Fe and oxygen. The peaks corresponding to the R1 and R2 discharge plateaus demonstrate a rapid decline, indicating the poor reversibility of the oxygen redox process. Similarly, the peak associated with the discharge plateau R3 shows a decreasing trend over cycling, indicating the limited reversibility of the Fe redox reaction. Similarly, the oxidation peaks also exhibit

a decrease in intensity over cycling, indicating the reduced participation of oxygen in the oxidation reaction and reflecting the high irreversibility of the reaction.

Figure 4d shows the cyclic voltammogram for the 2%-450 rpm-50 hour material within the voltage range of 1.5V to 4.8V. The CV curve exhibits two anodic peaks centered at 4.2V and 4.8, representing the presence of Fe and oxygen oxidation reaction respectively. Additionally, two cathodic peaks at around 2.19V and 3.1V, representing the corresponding Fe and oxygen reduction processes respectively. During prolonged cycling, the intensity of the oxygen oxidation peak at 4.8V and the oxygen reduction peak at 3.1 V exhibit a significant peak decrease, highlighting the limited reversibility of the oxygen redox reactions. Furthermore, the oxidation peak corresponding to the Fe, initially observed at 4.2 V, undergoes a gradual shift towards higher voltages and a decrease in intensity over cycling. Similarly, the reduction peak associated with the Fe, located at 2.19 V, also experiences a decline in intensity. These reductions in peak intensity, accompanied by a decrease in current density, indicate the presence of hysteresis, voltage fade, and capacity fade within the system.

Figure 4e and f display the XRD analysis results for the material with 2% cation vacancies at different milling times and rotational speeds. Upon examining the XRD pattern of the 2%-450 rpm-10 hour material, numerous impure phases are observed. Specifically, the first two peaks at around 33 and 36 degrees correspond to Fe_2O_3, indicating that Fe_2O_3 did not undergo the desired reaction.

By comparing the prominent peak at approximately 43 degrees in the 2% cation vacancies material with that of the material with 0% cation vacancies, it is evident that the peak intensity is higher, indicating the presence of the correct phase alongside a significant amount of Fe_2O_3. Conversely, the same peak in the material with 0% cation vacancies exhibits a lower intensity, suggesting a higher degree of Fe_2O_3 participation in the reaction. Additionally, as the milling time increases, similar to the material with 0% cation vacancies, more Fe_2O_3 becomes involved in the reaction, thereby reducing the presence of impure phases.

6% cation vacancies

The 6% cation vacancies ($Li_{1.1}Fe_{0.5}Nb_{0.28}O_2$) was prepared by dry milling at a rotational speed of 600 rpm for a total milling time of 50 hours.
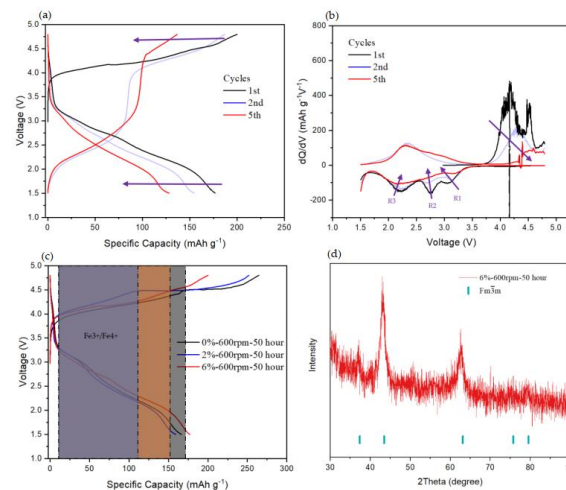

Figure 5 (a) Charge/discharge curve and the corresponding dQ/dV curve (b) of the 6%-600 rpm-50 hour material for the 5th cycle. (c) Charge/discharge curves of the initial cycle of the 0%-600 rpm-50 hour, 2%-600 rpm-50 hour and 6%-600 rpm-50 hour. (d) The XRD patterns of the 6%-600 rpm-50 hour material.

Upon analyzing the charge/discharge curve depicted in figure 5a, it is evident that the material with 6% cation vacancies exhibits the lowest charge-specific capacity, measuring 200 mAh g^{-1}. This capacity is lower compared to the materials with 0% and 2% cation vacancies. Furthermore, the material with 6% cation vacancies demonstrates a more substantial capacity fade over time, indicating poorer phase stability and reduced reversibility of redox reactions. The dQ/dV of the 6%-600 rpm-50 hour material in figure 5b highlights the irreversible nature of the oxygen reduction reaction, as evidenced by the rapid decrease in the peaks corresponding to the R1 and R2 discharge plateaus. Moreover, the peak related to the R3 discharge plateau, representing the reduction of Fe, shows a declining trend over cycling, indicating poor reversibility of the Fe redox reactions. This reduction in peak intensities helps explain the observed high capacity fading during cycling. Additionally, the poor reversibility of the oxygen redox process is represented by the decreasing trend of the oxidation peaks.

In the material with 6% cation vacancies, the first charge plateau (indicated by the shaded area) is relatively long compared to the material with 2% cation vacancies, as shown in figure 5c. This suggests that the material with 6% cation vacancies exhibits improved lithium conductivity, which can

influence the redox reaction in this voltage range. The improved Li diffusion can be explained by the XRD analysis.

Even in the extreme conditions of high rotational speed (600 rpm) and long milling time (50 hours), obtaining a super pure phase is still challenging with the 6% cation vacancies material. The XRD pattern in Figure 5d clearly indicates the presence of impurities, represented by peaks around 32 degrees, which indicate the presence of $LiNbO_3$. The high amount of Nb in the 6% cation vacancies material makes it difficult to form the desired phase, and instead, Nb tends to react with Li to form $LiNbO_3$, which is a lithium-poor phase compared to the disordered rock salt structure. Although $LiNbO_3$ exhibits better lithium conductivity, facilitating Li diffusion and explaining the longer plateau of Fe oxidation during the initial charge, it is not electrochemically active as it does not facilitate oxygen redox reactions. Therefore, while $LiNbO_3$ may have some benefits in terms of Li conductivity, it is not desirable from an electrochemical perspective. In conclusion, the process of building vacancies through this method needs further optimization to achieve a purer phase.

5. Conclusion

In conclusion, the mechanochemical ball milling process was successfully employed to design and synthesize various cation disordered Li-excess cathode oxides, both with and without cation vacancies. However, some impurities and poor crystallinity were observed in the synthesized materials. Among the materials synthesized using this technique, the 0%-600 rpm-50 hour material exhibited the highest initial charge capacity of approximately 260 mAh g^{-1}, while the 6%-600 rpm-50 hour material displayed the highest initial discharge capacity of around 177 mAh g^{-1}.

The significant capacity decline observed in the materials synthesized through dry milling indicates that this method does not result in the desired pure phase and introduces notable impurities. Consequently, these impurities have an adverse impact on the reversibility of transition metal redox reactions and the cycling stability of the material.

Furthermore, the introduction of cation vacancies through the dry milling technique leads to even poorer crystallinity, resulting in an unstable phase.

This instability is a contributing factor to the poor cycling stability observed in the materials with 2% and 6% cation vacancies. As a consequence, these materials exhibit significant capacity fade over cycling, further highlighting the impact of the unstable phase on their electrochemical performance.

The findings clearly indicate that the dry milling synthesis technique employed in this study is not optimal and requires further refinement and optimization. Moreover, the synthesis process should be optimized to incorporate vacancies in a controlled manner, ensuring an increase in capacity and improved overall performance.

References

[1] Placke, T., Kloepsch, R., Dühnen, S., & Winter, M. (2017). Lithium ion, lithium metal, and alternative rechargeable battery technologies: the odyssey for high energy density. Journal of Solid State Electrochemistry, 21, 1939-1964.

[2] Schmuch, R., Wagner, R., Hörpel, G., Placke, T., & Winter, M. (2018). Performance and cost of materials for lithium-based rechargeable automotive batteries. Nature Energy, 3(4), 267-278.

[3] Lee, J., Urban, A., Li, X., Su, D., Hautier, G., & Ceder, G. (2014). Unlocking the potential of cation-disordered oxides for rechargeable lithium batteries. science, 343(6170), 519-522.

[4] Urban, A., Lee, J., & Ceder, G. (2014). The configurational space of rocksalt-type oxides for high-capacity lithium battery electrodes. Advanced Energy Materials, 4(13), 1400478.

6. Acknowledgements